applied sciences

MDPI

Article

Effect of Interatomic Potential on Simulation of Fracture Behavior of Cu/Graphene Composite: A Molecular Dynamics Study

Liliya R. Safina [1], Elizaveta A. Rozhnova [2], Ramil T. Murzaev [1] and Julia A. Baimova [1,2,*]

[1] Institute for Metals Superplasticity Problems of RAS, Khalturina St., 39, Ufa 450001, Russia
[2] Physical-Technical Institute, Ufa University of Science and Technology, Zaki Validi St., 32, Ufa 450076, Russia
* Correspondence: julia.a.baimova@gmail.com

Abstract: Interatomic interaction potentials are compared using a molecular dynamics modeling method to choose the simplest, but most effective, model to describe the interaction of copper nanoparticles and graphene flakes. Three potentials are considered: (1) the bond-order potential; (2) a hybrid embedded-atom-method and Morse potential; and (3) the Morse potential. The interaction is investigated for crumpled graphene filled with copper nanoparticles to determine the possibility of obtaining a composite and the mechanical properties of this material. It is observed that not all potentials can be applied to describe the graphene–copper interaction in such a system. The bond-order potential potential takes into account various characteristics of the bond (for example, the angle of rotation and bond lengths); its application increases the simulation time and results in a strong interconnection between a metal nanoparticle and a graphene flake. The hybrid embedded-atom-method/Morse potential and the Morse potential show different results and lower bonding between graphene and copper. All the potentials enable a composite structure to be obtained; however, the resulting mechanical properties, such as strength, are different.

Keywords: crumpled graphene; Cu/graphene composite; molecular dynamics; interatomic potential

Citation: Safina, L.R.; Rozhnova, E.A.; Murzaev, R.T.; Baimova, J.A. Effect of Interatomic Potential on Simulation of Fracture Behavior of Cu/Graphene Composite: A Molecular Dynamics Study. *Appl. Sci.* **2023**, *13*, 916. https://doi.org/10.3390/app13020916

Academic Editors: Elena Korznikova and Andrey Kistanov

Received: 30 November 2022
Revised: 2 January 2023
Accepted: 4 January 2023
Published: 9 January 2023

1. Introduction

The development of new composites with improved mechanical properties composed of carbon structures and metal nanoparticles is of great importance. The combination of graphene with the most widespread metals, such as aluminum, nickel, copper, titanium, and silver, has been intensively studied over recent decades [1–4], is crumpled graphene (CG), which has recently been actively investigated for energy conservation applications [5,6]. The design of this lightweight three-dimensional graphene assembly and its mechanical properties were described in [7].

Copper (Cu) is widely used due to its inherent thermal conductivity and low cost [8]. Despite the widespread use of Cu, there is still a need to improve its mechanical, tribological, and thermal performance in various industries. Previously, it was established that graphene reinforcement of Cu increased its mechanical properties, while simultaneously maintaining high electrical conductivity [9]. It was shown that graphene decreased the thermal expansion coefficient compared to pure Cu, which is better for electronic applications [10–12]. Due to the improved tribological properties, copper-graphene composites have been proposed for use as coatings [13–15]. High strength and ductility were demonstrated for copper matrix composites within a graphene network [16–18].

The large-scale atomic/molecular massively parallel simulator (LAMMPS) can be used for any type of molecular dynamic (MD) simulation [2,5,14,19–35]. The MD simulation method is an effective tool for understanding the interconnection between the structure and properties of a material and the interactions between different structural elements [19,36–38]. For the MD simulation of graphene/metal interaction, a suitable interatomic potential must

be chosen to represent the particular issue under investigation. Interatomic potentials store basic information about the physical and chemical properties of the system [39,40]. On the one hand, it is very important to choose a potential that will describe the interaction between different materials as accurately as possible. On the other hand, computational costs need to be minimized. In large-scale atomistic modeling of complex systems, potentials, such as the analytical bond-order potential (BOP), the embedded atom method (EAM), and the Morse potential have been used successfully [20–22]. The simulation of Cu/graphene composites has also been conducted with more complicated potentials, such as the charge-optimized many-body potential (COMB) [41,42], for example, to study hydrocarbons on Cu surfaces [41] or the surface oxidation of Cu [43]. This potential has also been used to study graphene on a Cu surface with H and O atoms [23]. However, simulating interactions in graphene/metal systems remains challenging. The obtained adhesion energy, solubility, and catalytic properties of different metals in contact with carbon are quite different [44]. For example, the adhesion energy of graphene on a Cu substrate has been calculated experimentally as 0.72 J/m^2 [45] and 12.75 J/m^2 [46], and 0.40 J/m^2 [47] from first principles. In [48], the adhesion energy of graphene membranes on different substrates was measured experimentally at nano-scale using a nano-scratch method. The difference in system parameters is understandable since interatomic potentials have been developed to solve a range of problems, including graphene growth on a metal substrate, strengthening of a metal matrix by graphene coverage or graphene inclusions, and the study of thermal conductivity or mechanical properties. Even different atomic positioning of Me (shown for Ni) atoms on graphene surfaces results in different interactions [24,49]. For example, to obtain the potential parameters for the description of the interaction between a metal nanoparticle and graphene flake, it is better to consider a curved graphene surface (fullerene) interacting with a metal nanoparticle [50]. The specific energies of metal/graphene interfaces are very important and affect the resulting strength of the composite [51].

Since electronic decoupling between the metal and the graphene is observed for Cu, Ag and Au, the distance between metal and graphene is close to 3 Å, which is characteristic of van der Waals (vdW) interaction [52]. Thus, the interaction between Cu and graphene can be described by the pair interatomic potential, such as Lennard–Jones or Morse. These potentials can describe simple and noble metals, as well as carbon structures interacting with other elements [14,25–27,52,53].

A number of investigations have focused on analysis and comparison of interatomic potentials for carbon structures [28,54]. However, there is no consensus on the choice of potential for describing the interaction in systems such as carbon networks filled with metal nanoparticles. Thus, in the present study, three different potentials (BOP, EAM-Morse, and Morse) are compared to describe the Cu-C interaction. Using these potentials, the fabrication of composites based on copper nanoparticles and crumpled graphene and the investigation of their mechanical properties are considered.

2. Simulation Details

2.1. Interatomic Potential

For the graphene/Cu system, it is necessary to choose a potential that takes into account the covalent bonds in graphene, the interaction of Me atoms with graphene, and the interactions between Me atoms. The resulting potential function is defined as the sum of three potential energies for carbon-carbon E_{C-C}, carbon-copper E_{C-Cu} and copper-copper E_{Cu-Cu} interactions:

$$E_{system} = E_{C-C} + E_{C-Cu} + E_{Cu-Cu} \quad (1)$$

2.1.1. AIREBO Potential

The first term in (1) is calculated using the AIREBO potential, which includes both covalent bonds in the basal plane of graphene and van der Waals interactions between graphene flakes [55]:

$$E_{C-C} = \frac{1}{2}\sum_{i}\sum_{i\neq j}[E_{ij}^{REBO} + E_{ij}^{LJ} + \sum_{k\neq i,j}\sum_{l\neq i,j,k} E_{kijl}^{TORSION}], \quad (2)$$

where E_{ij}^{REBO} is the hydrocarbon REBO potential developed in [56], E_{ij}^{LJ} is for longer-range interactions using a form similar to the standard Lennard–Jones potential, and $E_{kijl}^{TORSION}$ describes changes in the dihedral angles. This potential was successfully used for the investigation of different carbon structures and their properties [5,29,57].

2.1.2. Morse Potential

To reproduce the graphene/Cu and Cu/Cu interaction, the Morse potential with parameters D_e = 0.3429 eV, R_e = 2.8660 Å and β = 1.3588 1/Å for Cu-Cu [58]; and D_e = −0.100 eV, R_e = 2.220 Å, β = 1.700 1/Å for Cu-C is chosen. For graphene/Cu, the cutoff distance is 6.5 Å. As graphene shows weak interaction with Cu [47,59–62], this enables use of simple pair interatomic potentials, such as Lennard–Jones or Morse [30,63], for such interactions.

$$E_{Cu-C}(r) = D_e[(1 - e^{-\beta(r-R_e)})^2 - 1], \quad (3)$$

where D_e is the binding energy, R_e is the equilibrium distance, and β is the potential parameter characterizing the bond strength.

The Morse potential has been used successfully to describe the interaction of metals with graphene and silicene [64], the interaction of atoms of the light elements C, N, O with atoms of the fcc metals Al, Ag and Ni [53], and the catalysis of nanotubes [65]. It was shown in [66] that the Morse potential provides a more precise and generalized description even for the simulation of covalent materials and surface interactions. Graphene/Me systems were also simulated with this potential [27,31,32,67,68].

2.1.3. EAM and Morse Potential

The second way to describe the graphene/Cu interaction is to use a hybrid EAM (embedded-atom-method) and the Morse potential. The realistic EAM potential, parameterized by Mendelev et al. [69], is used to describe the atomic interaction within Cu nanoparticles. It has been repeatedly shown that the EAM potential [70,71] accurately describes the interaction of many-body atoms in metallic systems and is widely used to model deformation behavior under various loading conditions [72–74]. To describe the Cu-C interaction, the Morse potential again is used.

2.1.4. BOP Potential

The bond-order potential (BOP) is based on the chemically intuitive tight-binding approximation and developed on the basis of quantum mechanical theory. Zhou et al. developed parameters for describing the C–Cu interaction that reasonably reflected the property trends of the important carbon phases [20]. This potential allows for the simulation of graphene growth on a Cu substrate.

The BOP potential, unlike the other two potentials described above, includes all three interactions at once: Cu-Cu, C-C, and Cu-C. The total energy of the BOP potential is given by

$$E = \frac{1}{2}\sum_{i=1}^{N}\sum_{j=i_1}^{i_N}[\phi_{cc}(r_{ij}) - \sum_{i=1}^{N}\sum_{j=i_1}^{i_N}\beta_{\sigma,cc}(r_{ij})\Theta_{\sigma,ij} - \sum_{i=1}^{N}\sum_{j=i_1}^{i_N}\beta_{\pi,cc}(r_{i,j}\Theta_{\pi,ij}], \quad (4)$$

where $\phi_{cc}(r_{ij})$, $\beta_{\sigma,cc}(r_{ij})$ and $\beta_{\pi,cc}(r_{i,j})$ are the electron density and the pair functions corresponding to σ and π couplings, respectively. Furthermore, $\Theta_{\sigma,ij}$ and $\Theta_{\pi,ij}$ are the multi-body functions corresponding to the neighboring atoms.

The BOP potential convincingly explains not only the growth of graphene, graphite, and carbon nanotube crystals, but also the transformation of graphite into diamond at high-pressure [20]. This potential has also been successfully used to study the sub-surface mechanical behavior of a nanocarbon particle with a diamond structure and a copper substrate upon nanocontact [33].

2.2. Initial Structure

Three different structures were investigated to confirm the application of each potential: (i) graphene with one Cu atom, (ii) curved graphene flake with Cu nanoparticle inside, and (iii) a composite precursor obtained from graphene flakes filled with nanoparticles. Initial structures for MD simulation were prepared using visual molecular dynamics (VMD) simulation and visualization software with custom Python code.

The melting temperature for Cu can be checked to verify the potential function. To find the melting temperature, Cu nanoparticles with diameter 7 Å were heated at a temperature from 0 K to 2000 K, with a heating rate of 50 K/ps. In Table 1, the melting temperature of Cu nanoparticles obtained with different potentials is presented. Consistent with the observations reported in [75], the average melting temperature was 723 K. It should be noted that, for such small nanoparticles, the melting temperature depends substantially on the particle size.

It was also found that the presence of a graphene flake near a nanoparticle can slow down the melting of the Cu nanoparticle. It was found that, if a graphene flake with the nanoparticle on its surface is examined in a quite large simulation cell, the Cu nanoparticle in the course of heating will move far from the graphene plane and melt at the same temperature as a single nanoparticle. However, when the nanoparticle was already covered with graphene (as it would be in a 3D structure composed of a number of flakes and nanoparticles), the melting temperature of the Cu nanoparticle increased to 1000 to 1300 K. Similar results were previously obtained in [23]. However, for comparison with the literature, only the melting temperature of pure Cu nanoparticles is presented.

For the system composed of a graphene flake and a Cu atom, the equilibrium distance between the graphene and the Cu atom is defined as h and was found to be 3.2 Å for the BOP potential and 6.4 Å for the EAM-Morse and Morse potentials. For comparison, results from the literature are presented in Table 1. To understand this very significant difference, the potential energy of the system as a function of the distance between a Cu atom and graphene was investigated. Since the BOP potential was designed specifically for growing graphene on a Cu substrate [75], it reproduces strong bonding between graphene and copper. Therefore, when simulating the interaction of one copper atom on the surface of graphene (the initial distance between a Cu atom and graphene is 3 Å), the equilibrium state in the system is already reached at a distance of 3.2 Å and the potential energy ceases to change right at the beginning since, in the initial state, the Cu atom is already close to the graphene surface. However, the Morse potential reproduces a very neutral interaction between Cu and graphene. As reported in the literature [47,59], the binding energy for Cu and graphene is not high in comparison with metals such as Al, Ni, etc. This is why, when the potential energy as a function of distance is calculated using the Morse and EAM-Morse potentials, in both cases the Cu atom moves away from graphene to a distance of up to 6.4Å during the first simulation steps. The potential energy in the system with BOP potential is higher than for the Morse and Morse-EAM potentials, which is also understandable from the point of view of reproducing the strong bonding. It should also be noted that the results of an interaction between one Cu atom and graphene are very different from the results for an interaction of a Cu nanoparticle and one graphene flake, and for interaction in 3D graphene filled with Cu nanoparticles, which is discussed further below.

In Figure 1a, one graphene flake is shown at the initial state and after exposure at 300 K, simulated with the help of different potential functions. The behavior under exposure is discussed further below.

Table 1. Melting temperature of Cu nanoparticle T_m and equilibrium distance between Cu atom and graphene layer h obtained with different methods.

	BOP	EAM-Morse	Morse	BOP [75]	Experiment [20]
T_m, K	830	797	730	723	–
h, Å	3.2	6.4	6.4	–	3.2

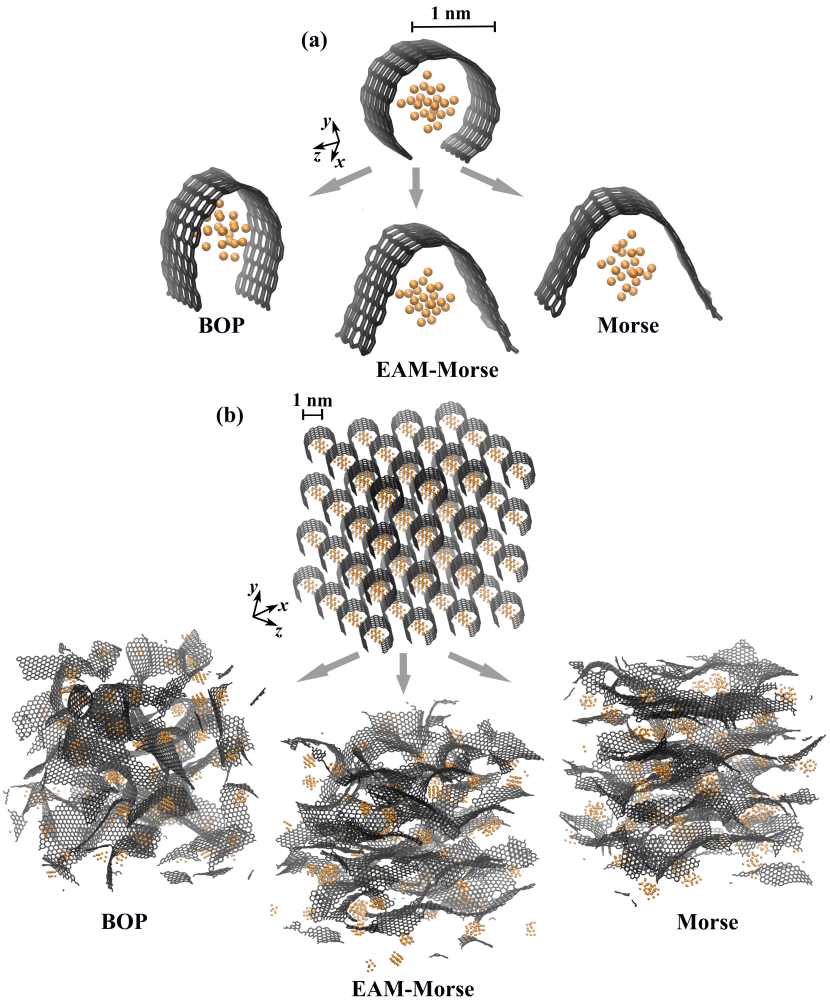

Figure 1. (**a**) Graphene flake with Cu nanoparticle inside and (**b**) composite precursor at the initial state and after exposure at 300 K. Cu atoms are shown in orange and C atoms are shown in black color.

To obtain a composite, one GF filled with nanoparticles was rotated and repeated along the *x*-, *y*-, and *z*-axes to obtain a 3D structure. The composite precursor is presented in Figure 1b at the initial state and after exposure at 300 K, simulated with the help of different potential functions. The size of the simulation cell at the initial state was $10.1 \times 10.0 \times 8.4$ nm. The exposure process is discussed further below. Then, hydrostatic compression was used to reduce large pores between the individual elements of the composite precursor. The structures were compressed to approximately the same size: $4.2 \times 4.2 \times 4.2$ nm. Then, hydrostatic compression was used to obtain the composite with the maximum possible densities. Hydrostatic compression was applied with a strain rate of $\dot{\varepsilon} = 0.01$ ps^{-1}. Details of the structure fabrication are presented in [2,27]. For simplicity, the results for a structure

obtained with the BOP potential are referred to as CG-Cu$_{BOP}$, with the hybrid EAM-Morse potential as CG-Cu$_{EM}$, and with the Morse potential as CG-Cu$_{M}$.

The structures were studied at a constant temperature to trace the dynamics of the interaction of Cu nanoparticles with graphene using different potentials. The simulation was conducted using a large-scale atomic/molecular massively parallel simulator (LAMMPS). Equations of motion for the atoms were integrated numerically using the fourth-order Verlet method with a time step of 0.1 fs. A Nose–Hoover thermostat was used to control the system temperature. The periodic boundary conditions were applied in all directions.

To study the mechanical properties of the composites, uniaxial tension was applied along the x-axis, with a strain rate of 0.005 ps^{-1}.

3. Results

3.1. Exposure

Let us first consider the exposure of a single flake at 300 K. Even at this stage of simulation, a difference in the behavior of nanoparticles in contact with a graphene flake simulated with different potentials is observed. As can be seen from Figure 1a, the behavior of a Cu nanoparticle inside GF for the EAM-Morse and Morse potentials is very similar and quite different from that for GF simulated with the BOP potential. When a GF is simulated with the BOP potential, the Cu nanoparticle attracts the sides of graphene, while for a GF simulated with the EAM-Morse and Morse potential, the Cu nanoparticle repulses the sides of the GF. It can also be seen that, with the use of the EAM potential, the Cu nanoparticle preserves the crystalline order better than with the BOP and pure Morse potentials. The Cu nanoparticle inside GF simulated with the BOP potential changes its shape to become more spherical. However, for a single GF it is seen that the interaction of Cu and GF is weaker than within Cu atoms in the nanoparticle and the GF is opened as for the Morse potential.

From Figure 1b, it can be seen that Cu nanoparticles simulated with BOP are attracted to GFs. In contrast, for composite precursors simulated with the EAM-Morse and Morse potentials, Cu nanoparticles move in opposite directions from GFs, interact with each other or coagulate. For all three cases, GFs open, but for CG-Cu$_{BOP}$, GFs with attached Cu nanoparticles can be seen, while, for CG-Cu$_{EM}$ and CG-Cu$_{M}$, there are graphene layers with coagulated nanoparticles. The behavior of the structure simulated with the BOP potential can be explained by the fact that this potential was developed to investigate the growth of graphene on a copper substrate and, therefore, in this case, the strongest bond between a graphene flake and a copper nanoparticle is expressed [20]. Potential parameters were chosen to reproduce graphene adsorption on Cu and, consequently, the C-Cu interaction is much stronger than the simple van der Waals interaction. Moreover, in contrast to AIREBO used with the EAM-Morse and Morse potentials, the BOP potential results in worse interaction between GFs—the GFs are rotated more randomly during exposure. Use of AIREBO results in the formation of layered structures and more curved GFs.

As was mentioned in Section 2, the results for one Cu atom and graphene showed a significant difference in the distance between the Cu atom and graphene for the BOP and Morse potentials. It can be concluded that there is no connection to the interaction between one Cu atom with graphene and the interaction of the number of graphene flakes and Cu nanoparticles. We started with simulation of graphene and one Cu atom to obtain a better understanding of this difference. It can initially be concluded that, for separate Cu atoms and one graphene plane, or for a Cu substrate and separate C atoms, it is better to use the BOP potential. However, when we try to understand the complex system composed of crumpled graphene flakes and Cu nanoparticles, we do not need to reproduce such strong adhesion. If we move from a system composed of a Cu atom and graphene to a system composed of nanoparticles and graphene flake, we see very different behavior—nanoparticles do not move so far from the flake. Here, the Morse potential is much more suitable, leading to the conclusion that different potentials can be used to solve different problems.

3.2. Hydrostatic Compression

As mentioned in Section 2, the composite precursor was hydrostatically compressed to obtain zero stresses in the system. Then, it was hydrostatically compressed at 1000 K to obtain a composite with maximal densities of 5.69 g/cm^3 (BOP), 5.59 (EAM-Morse) and 5.64 (Morse). In Figure 2a, snapshots of the composite precursor, obtained with three different potential functions, are presented after exposure at 300 K, followed by hydrostatic compression to the state with zero stress. In Figure 2b,c, pressure (b) and potential energy (c) as a function of compression strain are presented during hydrostatic compression at 1000 K. In Figure 2d, snapshots of the composite obtained with three different potential functions are presented.

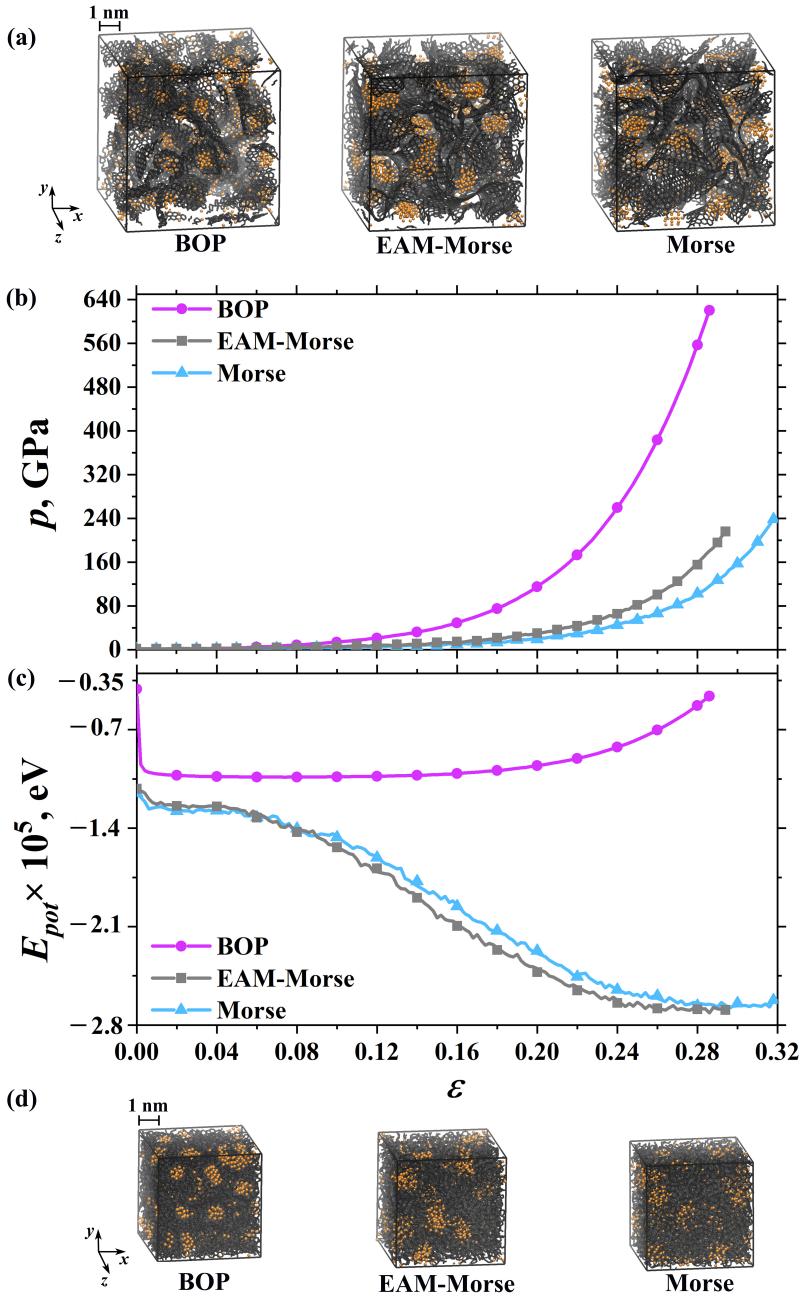

Figure 2. (**a**) Snapshots of the composite precursors obtained with different potentials after exposure at 300 K followed by hydrostatic compression. (**b**,**c**) Pressure and potential energy changes during hydrostatic compression. (**d**) Snapshots of the composite, obtained with different potentials. Cu atoms are shown in orange and C atoms are shown in black.

As is shown in Figure 2a, after pre-compression, in the structure obtained with the EAM-Morse and Morse potentials, the Cu nanoparticles coagulate. For structure σ obtained with the BOP potential, the Cu nanoparticles are covered with GFs, which occurred during exposure and was enhanced during pre-compression. Thus, we have something like graphene "balls" with nanoparticles inside.

For all three cases, it was found that, with increase in strain, the pressure increased rapidly (see Figure 2b), which is common for graphene networks under compression [34]. However, for CG-Cu_{BOP}, the maximum stress was 650 GPa, while for CG-Cu_{EM} and CG-Cu_{M}, it was almost two times lower. This difference can be explained by the fact that the BOP potential somehow makes both the graphene and the nanoparticles more rigid and, therefore, greater pressure is required to compress the structure.

By comparison of Figure 2b,c, it can be seen that, before $\varepsilon = 0.08$ (BOP) and $\varepsilon = 0.04$ (EAM-Morse, Morse), the potential energy is almost unchanged and the stress is close to zero. Before these values of strain, there are still many pores in the composite precursor and the neighboring elements interact weakly with each other. After $\varepsilon = 0.08$ ($\varepsilon = 0.04$), the GF begins to interact and new covalent bonds appear between the GFs. Thus, the separated graphene elements transform into a graphene network. The curves for the structure obtained with the EAM-Morse and Morse potentials are very close, both for $\sigma(\varepsilon)$ and $E_{pot}(\varepsilon)$. The main difference is that, for the structure simulated with BOP, the potential energy increases, while for the EAM-Morse and Morse potentials, it decreases. This can be explained as a result of the BOP potential causing both the Cu nanoparticles and graphene flakes to become more rigid. Consequently, in the process of hydrostatic compression, due to the high rigidity of the nanoparticles and graphene, the potential energy in the system increases. For use of the other two potentials, the copper nanoparticles, in this case, are softer; in addition, the AIREBO potential enables graphene to bend more easily and, thus, hydrostatic compression occurs much more easily.

This is also connected with the simulation process itself. It should be noted that compression with the EAM-Morse and Morse potentials stopped automatically when the structure compressed to a quite high density and physically could not be compressed further. However, for compression with BOP, the structure could be compressed to an unrealistic density and stopped manually when an average density 5.6 g/cm^3 was achieved. This was also confirmed by the constant increase in the potential energy during compression. For the Morse potential, compression resulted in the transformation of the system to a low-energy state since AIREBO enabled crumpling of graphene and softening of the Cu nanoparticles. Several processes decreased the potential energy: coagulation of the nanoparticles, decrease in the space between the separated elements, coverage of nanoparticles by graphene flakes, and the appearance of new bonds between neighboring flakes. In the structure simulated with the BOP potential, it was closer to the situation in which a system of rigid "balls" and rigid flakes are compressed, which increases the energy of the system.

The deformation behavior of a single element of the composite was also analyzed. For CG-Cu_{BOP}, even under high-temperature compression, the crystalline order of nanoparticles remained. For CG-Cu_{EM} and CG-Cu_{M}, the metal nanoparticles melted, which contributed to easier deformation and the formation of new chemical bonds. In [75], it was reported that the melting temperature of Cu nanoparticles was 723 K, which was lower than the hydrostatic compression temperature of 1000 K. Thus, the results obtained with the BOP potential contradict even the melting temperature of Cu. It has previously been reported that graphene flakes deform more easily under high-temperature hydrostatic compression than at room temperature [22,35,76].

3.3. Uniaxial Tension

The stress-strain curves for the composites obtained with different potentials are presented in Figure 3. Again, the results observed for the CG-Cu_{BOP} composite were different from the other two potentials. Analysis showed that the elastic regime can be

defined before ε = 0.06 for all structures (see the insert in Figure 3). After this, the slope of the curve changes, though is still close to a linear regime. The transition to the plastic deformation took place at higher stresses (about 90 GPa) for CG-Cu$_{BOP}$ in comparison to CG-Cu$_{EM}$ and CG-Cu$_{M}$ (which were about 60 GPa). The elastic modulus obtained with the EAM-Morse and Morse potentials were very close −267 and 268 GPa, while, for composite fabricated with the BOP potential, the elastic modulus was almost two times higher −487 GPa.

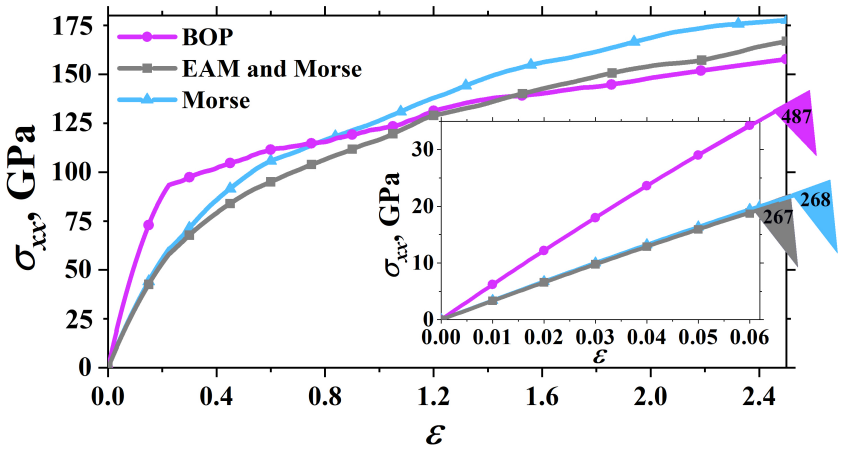

Figure 3. Stress-strain curves for composites under tension. The insertion shows the elastic regime and elastic modulus.

The stress-strain curves for CG-Cu$_{EM}$ and CG-Cu$_{M}$ are coincident up to ε = 0.22. Since the Morse potential is used in these two structures to describe the Cu-C interaction, the only difference is in the description of the Cu nanoparticles. Therefore, these curves are in good agreement. It is also important to note that, for all three structures, the transition from elastic to plastic deformation occurred at ε = 0.22. This is not the maximum value since the composite can be stretched further. However, in the present investigation, the main goal was to understand the effect of the potential function used on the process of composite fabrication.

It should be noted that all the obtained composites had high strength and ductility. After ε = 0.8, the stress-strain curves for all the composites were very close; no fracture took place before ε = 2.5.

In Figure 4, the distribution of Cu atoms in the composite before (ε = 0.0) and after tension (at final state ε = 2.5), and in the graphene network, are presented separately.

After compression for CG-Cu$_{BOP}$, the Cu nanoparticles remained almost the same as after exposure, occurring as spherical particles of an approximately round shape. In comparison, for CG-Cu$_{M}$, already melted nanoparticles and Cu atoms were spread over the structure. Since EAM resulted in higher interaction energy for Cu-Cu, Cu nanoparticles can still be seen in the structure, but already melted, or pre-melted.

For CG-Cu$_{BOP}$ obtained with the BOP potential, the metal nanoparticles remained in a crystalline order and appeared as metal clusters with a size larger than the initial state. Even during tension, the Cu nanoparticles interacted and coagulated to form bigger clusters. Cavities for the Cu nanoparticles can be seen in the snapshots of the graphene network. For CG-Cu$_{EM}$ and CG-Cu$_{M}$, the Cu atoms were almost uniformly distributed in the graphene network during tension, spreading over the graphene flakes in both cases. This resulted in the formation of a more uniform graphene network.

It can be concluded that the main difference in the results obtained with the BOP and EAM-Morse/Morse potentials was observed in the elastic regime. The composites obtained from the graphene networks filled with Cu nanoparticles are very promising because they show high strength and ductility. However, different treatment temperatures should be considered for the development of composite fabrication under hydrostatic compression.

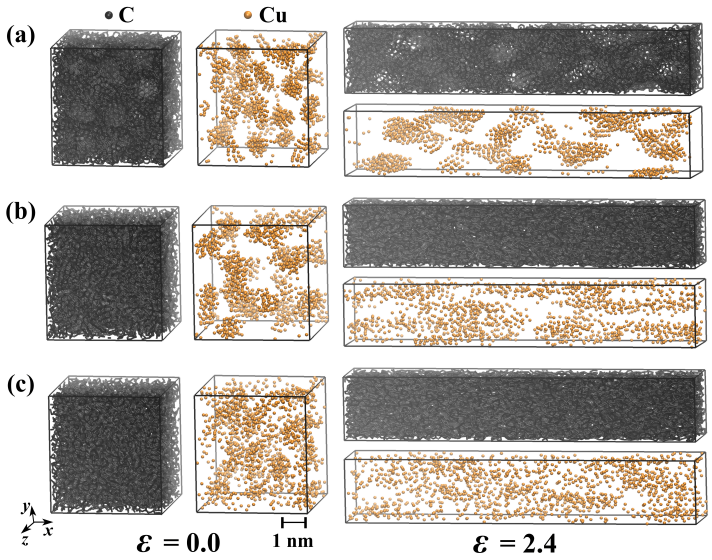

Figure 4. Copper atoms (orange color) and graphene network (black color) are shown separately before and after uniaxial tension: (**a**) BOP; (**b**) EAM-Morse; and (**c**) Morse. Colors as in Figure 1.

4. Conclusions

A molecular dynamics approach was used to simulate the deformation behavior and mechanical properties of a Cu/graphene nanocomposite composed of a graphene network and Cu nanoparticles. How the potential used to represent the atomic interactions affected the final composite structure and deformation behavior was analyzed. BOP, EAM-Morse, and Morse potentials were investigated in the present study.

One of the purposes of the present study was to determine the most suitable potential for the simulation of the interaction between Cu and graphene in the composites and to identify which potential would make the simulation easier, more efficient, and more accurate. Although the BOP potential was able to accurately reproduce the interatomic interaction between C and Cu, it was found to be more suitable for the simulation of graphene growth on a Cu substrate than for the study of Cu/graphene composites. It was found that the Cu nanoparticles did not melt during high-temperature compression, while the melting temperature of Cu nanoparticles was quite low. Moreover, the EAM-Morse and Morse potentials gave approximately the same results for a much lower simulation time in comparison with the BOP potential. The same results were obtained for Ni nanoparticles in a graphene network where the complex ReaxFF potential was compared with the Morse potential [22]. Therefore, for the simulation of a large number of atoms, it is better to use a simple Morse potential.

Author Contributions: Conceptualization, J.A.B.; methodology, L.R.S.; formal analysis, E.A.R.; resources, R.T.M.; investigation, L.R.S.; writing—original draft preparation, L.R.S., J.A.B. and R.T.M. All authors have read and agreed to the published version of the manuscript.

Funding: The work of J.A.B., R.T.M. and E.A.R. is supported by the State Assignment of IMSP RAS (Young Scientist Laboratory). The work of L.R.S. is supported by a grant for young scientists provided by the Republic of Bashkortostan.

Institutional Review Board Statement: Not applicable.

Informed Consent Statement: Not applicable.

Data Availability Statement: The data presented in this study are available on request from the corresponding author. The data are not publicly available due to the work is not finished yet.

Conflicts of Interest: The authors declare no conflict of interest.

References

1. Wang, X.; Xiao, W.; Wang, J.; Sun, L.; Shi, J.; Guo, H.; Liu, Y.; Wang, L. Enhanced interfacial strength of graphene reinforced aluminum composites via X (Cu, Ni, Ti)-coating: Molecular-dynamics insights. *Adv. Powder Technol.* **2021**, *32*, 2585–2590. [CrossRef]
2. Safina, L.R.; Baimova, J.A.; Krylova, K.A.; Murzaev, R.T.; Shcherbinin, S.A.; Mulyukov, R.R. Ni–Graphene Composite Obtained by Pressure–Temperature Treatment: Atomistic Simulations. *Phys. Status Solidi (RRL)–Rapid Res. Lett.* **2021**, *15*, 2100429. [CrossRef]
3. Hou, B.; Liu, P.; Wang, A.; Xie, J. Interface optimization strategy for enhancing the mechanical and thermal properties of aligned graphene/Al composite. *J. Alloys Compd.* **2022**, *900*, 163555. [CrossRef]
4. Wang, M.; Sheng, J.; Wang, L.D.; Wang, G.; Fei, W.D. Achieving high strength and electrical properties in drawn fine Cu matrix composite wire reinforced by in-situ grown graphene. *J. Mater. Res. Technol.* **2022**, *17*, 3205–3210. [CrossRef]
5. Krylova, K.; Baimova, J.; Mulyukov, R. Effect of deformation on dehydrogenation mechanisms of crumpled graphene: Molecular dynamics simulation. *Lett. Mater.* **2019**, *9*, 81–85. [CrossRef]
6. Mathew, E.E.; Balachandran, M. Crumpled and porous graphene for supercapacitor applications: A short review. *Carbon Lett.* **2021**. [CrossRef]
7. Qin, Z.; Jung, G.S.; Kang, M.J.; Buehler, M.J. The mechanics and design of a lightweight three-dimensional graphene assembly. *Sci. Adv.* **2017**, *3*, e1601536. [CrossRef]
8. Wu, M.; Chen, Z.; Huang, C.; Huang, K.; Jiang, K.; Liu, J. Graphene platelet reinforced copper composites for improved tribological and thermal properties. *RSC Adv.* **2019**, *9*, 39883–39892. [CrossRef]
9. Chen, D.; Feng, H.; Li, J. Graphene Oxide: Preparation, Functionalization, and Electrochemical Applications. *Chem. Rev.* **2012**, *112*, 6027–6053. [CrossRef]
10. Wejrzanowski, T.; Grybczuk, M.; Chmielewski, M.; Pietrzak, K.; Kurzydlowski, K.; Strojny-Nedza, A. Thermal conductivity of metal-graphene composites. *Mater. Des.* **2016**, *99*, 163–173. [CrossRef]
11. Guo, S.; Zhang, X.; Shi, C.; Zhao, D.; Liu, E.; He, C.; Zhao, N. Comprehensive performance regulation of Cu matrix composites with graphene nanoplatelets in situ encapsulated Al2O3 nanoparticles as reinforcement. *Carbon* **2022**, *188*, 81–94. [CrossRef]
12. Ali, S.; Ahmad, F.; Yusoff, P.S.M.M.; Muhamad, N.; Oñate, E.; Raza, M.R.; Malik, K. A review of graphene reinforced Cu matrix composites for thermal management of smart electronics. *Compos. Part A Appl. Sci. Manuf.* **2021**, *144*, 106357. [CrossRef]
13. Zhai, W.; Lu, W.; Chen, Y.; Liu, X.; Zhou, L.; Lin, D. Gas-atomized copper-based particles encapsulated in graphene oxide for high wear-resistant composites. *Compos. Part B Eng.* **2019**, *157*, 131–139. [CrossRef]
14. Zhang, J.; Xu, Q.; Gao, L.; Ma, T.; Qiu, M.; Hu, Y.; Wang, H.; Luo, J. A molecular dynamics study of lubricating mechanism of graphene nanoflakes embedded in Cu-based nanocomposite. *Appl. Surf. Sci.* **2020**, *511*, 145620. [CrossRef]
15. Lin, G.; Peng, Y.; Dong, Z.; Xiong, D.B. Tribology behavior of high-content graphene/nanograined Cu bulk composites from core/shell nanoparticles. *Compos. Commun.* **2021**, *25*, 100777. [CrossRef]
16. Zhang, X.; Xu, Y.; Wang, M.; Liu, E.; Zhao, N.; Shi, C.; Lin, D.; Zhu, F.; He, C. A powder-metallurgy-based strategy toward three-dimensional graphene-like network for reinforcing copper matrix composites. *Nat. Commun.* **2020**, *11*, 2775. [CrossRef]
17. Shi, L.; Liu, M.; Yang, Y.; Liu, R.; Zhang, W.; Zheng, Q.; Ren, Z. Achieving high strength and ductility in copper matrix composites with graphene network. *Mater. Sci. Eng. A* **2021**, *828*, 142107. [CrossRef]
18. Shi, L.; Liu, M.; Zhang, W.; Ren, W.; Zhou, S.; Zhou, Q.; Yang, Y.; Ren, Z. Interfacial Design of Graphene Nanoplate Reinforced Copper Matrix Composites for High Mechanical Performance. *JOM* **2022**, *74*, 3082–3090. [CrossRef]
19. Savin, A.V. Multistability of Carbon Nanotube Packings on Flat Substrate. *Phys. Status Solidi (RRL)–Rapid Res. Lett.* **2021**, *16*, 2100437. [CrossRef]
20. Zhou, X.W.; Ward, D.K.; Foster, M.E. An analytical bond-order potential for carbon. *J. Comput. Chem.* **2015**, *36*, 1719–1735. [CrossRef]
21. Yan, Y.; Lei, Y.; Liu, S. Tensile responses of carbon nanotubes-reinforced copper nanocomposites: Molecular dynamics simulation. *Comput. Mater. Sci.* **2018**, *151*, 273–277. [CrossRef]
22. Safina, L.L.; Baimova, J.A. Molecular dynamics simulation of fabrication of Ni-graphene composite: Temperature effect. *Micro Nano Lett.* **2020**, *15*, 176–180. [CrossRef]
23. Klaver, T.; Zhu, S.E.; Sluiter, M.; Janssen, G. Molecular dynamics simulation of graphene on Cu (1 0 0) and (1 1 1) surfaces. *Carbon* **2015**, *82*, 538–547. [CrossRef]
24. Montazeri, A.; Panahi, B. MD-based estimates of enhanced load transfer in graphene/metal nanocomposites through Ni coating. *Appl. Surf. Sci.* **2018**, *457*, 1072–1080. [CrossRef]
25. Zhang, C.; Lu, C.; Pei, L.; Li, J.; Wang, R. The wrinkling and buckling of graphene induced by nanotwinned copper matrix: A molecular dynamics study. *Nano Mater. Sci.* **2021**, *3*, 95–103. [CrossRef]
26. Shuang, F.; Aifantis, K.E. Dislocation-graphene interactions in Cu/graphene composites and the effect of boundary conditions: A molecular dynamics study. *Carbon* **2021**, *172*, 50–70. [CrossRef]
27. Safina, L.R.; Krylova, K.A.; Baimova, J.A. Molecular dynamics study of the mechanical properties and deformation behavior of graphene/metal composites. *Mater. Today Phys.* **2022**, *28*, 100851. [CrossRef]
28. De Tomas, C.; Suarez-Martinez, I.; Marks, N.A. Graphitization of amorphous carbons: A comparative study of interatomic potentials. *Carbon* **2016**, *109*, 681–693. [CrossRef]

29. Rozhkov, M.; Abramenko, N.; Kolesnikova, A.; Romanov, A. Zero misorientation interfaces in graphene. *Lett. Mater.* **2020**, *10*, 551–557. [CrossRef]
30. Hong, Y.; Li, L.; Zeng, X.C.; Zhang, J. Tuning thermal contact conductance at graphene–copper interface *via* surface nanoengineering. *Nanoscale* **2015**, *7*, 6286–6294. [CrossRef]
31. Krylova, K.A.; Safina, L.R.; Murzaev, R.T.; Baimova, J.A.; Mulyukov, R.R. Effect of Nanoparticle Size on the Mechanical Strength of Ni–Graphene Composites. *Materials* **2021**, *14*, 3087. [CrossRef] [PubMed]
32. Yang, Y.; Liu, M.; Du, J.; Zhang, W.; Zhou, S.; Ren, W.; Zhou, Q.; Shi, L. Construction of graphene network in Ni matrix composites: A molecular dynamics study of densification process. *Carbon* **2022**, *191*, 55–66. [CrossRef]
33. Goh, B.; Choi, J. Mechanical evaluation of bidirectional surface deformation in contact between nanometer-sized carbon particle and copper substrate: A molecular dynamics approach. *Surfaces Interfaces* **2021**, *26*, 101388. [CrossRef]
34. Baimova, Y.A.; Murzaev, R.T.; Dmitriev, S.V. Mechanical properties of bulk carbon nanomaterials. *Phys. Solid State* **2014**, *56*, 2010–2016. [CrossRef]
35. Safina, L.; Baimova, J.; Krylova, K.; Murzaev, R.; Mulyukov, R. Simulation of metal-graphene composites by molecular dynamics: A review. *Lett. Mater.* **2020**, *10*, 351–360. [CrossRef]
36. Wang, X.; Feng, S.; Qi, L.; Gao, W.; Zhang, S. Mechanical properties of Cu50Zr50 amorphous/B2-CuZr crystalline composites studied by molecular dynamic method. *J. Non-Cryst. Solids* **2021**, *568*, 120942. [CrossRef]
37. Yang, Z.; Guo, Z.; Yuan, C.; Bai, X. Tribological behaviors of composites reinforced by different functionalized carbon nanotube using molecular dynamic simulation. *Wear* **2021**, *476*, 203669. [CrossRef]
38. Savin, A.V.; Savina, O.I. Elastic and Plastic Deformations of Carbon Nanotubes Multilayer Packing on a Flat Substrate. *J. Exp. Theor. Phys.* **2022**, *134*, 60–68. [CrossRef]
39. Zhou, K.; Liu, B.; Cai, Y.; Dmitriev, S.V.; Li, S. Modelling of Low-dimensional Functional Nanomaterials. *Phys. Status Solidi (RRL)–Rapid Search Lett.* **2022**, *16*, 2100654. [CrossRef]
40. Morkina, A.Y.; Tuvalev, I.I.; Dmitriev, S.V.; Bebikhov, Y.V.; Semenov, A.S.; Sharapova, Y.R. The selection of interatomic potentials for simulation of extreme actions within the tungsten lattice. *Front. Mater. Technol.* **2022**, 16–24. [CrossRef]
41. Liang, T.; Devine, B.; Phillpot, S.R.; Sinnott, S.B. Variable Charge Reactive Potential for Hydrocarbons to Simulate Organic-Copper Interactions. *J. Phys. Chem. A* **2012**, *116*, 7976–7991. [CrossRef] [PubMed]
42. Liang, T.; Shan, T.R.; Cheng, Y.T.; Devine, B.D.; Noordhoek, M.; Li, Y.; Lu, Z.; Phillpot, S.R.; Sinnott, S.B. Classical atomistic simulations of surfaces and heterogeneous interfaces with the charge-optimized many body (COMB) potentials. *Mater. Sci. Eng. R Rep.* **2013**, *74*, 255–279. [CrossRef]
43. Devine, B.; Shan, T.R.; Cheng, Y.T.; McGaughey, A.J.H.; Lee, M.; Phillpot, S.R.; Sinnott, S.B. Atomistic simulations of copper oxidation and Cu/CuO interfaces using charge-optimized many-body potentials. *Phys. Rev. B* **2011**, *84*, 125308. [CrossRef]
44. Elliott, J.A.; Shibuta, Y.; Amara, H.; Bichara, C.; Neyts, E.C. Atomistic modelling of CVD synthesis of carbon nanotubes and graphene. *Nanoscale* **2013**, *5*, 6662. [CrossRef]
45. Yoon, S.M.; Choi, W.M.; Baik, H.; Shin, H.J.; Song, I.; Kwon, M.S.; Bae, J.J.; Kim, H.; Lee, Y.H.; Choi, J.Y. Synthesis of Multilayer Graphene Balls by Carbon Segregation from Nickel Nanoparticles. *ACS Nano* **2012**, *6*, 6803–6811. [CrossRef]
46. Das, S.; Lahiri, D.; Lee, D.Y.; Agarwal, A.; Choi, W. Measurements of the adhesion energy of graphene to metallic substrates. *Carbon* **2013**, *59*, 121–129. [CrossRef]
47. Xu, Z.; Buehler, M.J. Interface structure and mechanics between graphene and metal substrates: A first-principles study. *J. Phys. Condens. Matter* **2010**, *22*, 485301. [CrossRef] [PubMed]
48. Lahiri, I.; Lahiri, D.; Jin, S.; Agarwal, A.; Choi, W. Carbon Nanotubes: How Strong Is Their Bond with the Substrate? *ACS Nano* **2011**, *5*, 780–787. [CrossRef]
49. Moseler, M.; Cervantes-Sodi, F.; Hofmann, S.; Csányi, G.; Ferrari, A.C. Dynamic Catalyst Restructuring during Carbon Nanotube Growth. *ACS Nano* **2010**, *4*, 7587–7595. [CrossRef]
50. Katin, K.P.; Prudkovskiy, V.S.; Maslov, M.M. Molecular dynamics simulation of nickel-coated graphene bending. *Micro Nano Lett.* **2018**, *13*, 160–164. [CrossRef]
51. Sheinerman, A. Modeling of structure and interface controlled strength of laminated metal/graphene composites. *Mech. Mater.* **2021**, *158*, 103888. [CrossRef]
52. Rezaei, R.; Deng, C.; Tavakoli-Anbaran, H.; Shariati, M. Deformation twinning-mediated pseudoelasticity in metal–graphene nanolayered membrane. *Philos. Mag. Lett.* **2016**, *96*, 322–329. [CrossRef]
53. Poletaev, G.; Zorya, I.; Rakitin, R.; Iliina, M. Interatomic potentials for describing impurity atoms of light elements in fcc metals. *Mater. Phys. Mech.* **2019**, *42*. [CrossRef]
54. Zalizniak, V.E.; Zolotov, O.A. Efficient embedded atom method interatomic potential for graphite and carbon nanostructures. *Mol. Simul.* **2017**, *43*, 1480–1484. [CrossRef]
55. Stuart, S.J.; Tutein, A.B.; Harrison, J.A. A reactive potential for hydrocarbons with intermolecular interactions. *J. Chem. Phys.* **2000**, *112*, 6472–6486. [CrossRef]
56. Brenner, D.W.; Shenderova, O.A.; Harrison, J.A.; Stuart, S.J.; Ni, B.; Sinnott, S.B. A second-generation reactive empirical bond order (REBO) potential energy expression for hydrocarbons. *J. Phys. Condens. Matter* **2002**, *14*, 783–802. [CrossRef]
57. Umeno, Y.; Yachi, Y.; Sato, M.; Shima, H. On the atomistic energetics of carbon nanotube collapse from AIREBO potential. *Phys. E -Low-Dimens. Syst. Nanostruct.* **2019**, *106*, 319–325. [CrossRef]

58. Girifalco, L.A.; Weizer, V.G. Application of the Morse Potential Function to Cubic Metals. *Phys. Rev.* **1959**, *114*, 687–690. [CrossRef]
59. Giovannetti, G.; Khomyakov, P.A.; Brocks, G.; Karpan, V.M.; van den Brink, J.; Kelly, P.J. Doping Graphene with Metal Contacts. *Phys. Rev. Lett.* **2008**, *101*, 026803. [CrossRef]
60. He, R.; Zhao, L.; Petrone, N.; Kim, K.S.; Roth, M.; Hone, J.; Kim, P.; Pasupathy, A.; Pinczuk, A. Large Physisorption Strain in Chemical Vapor Deposition of Graphene on Copper Substrates. *Nano Lett.* **2012**, *12*, 2408–2413. [CrossRef]
61. Nieto, A.; Bisht, A.; Lahiri, D.; Zhang, C.; Agarwal, A. Graphene reinforced metal and ceramic matrix composites: A review. *Int. Mater. Rev.* **2016**, *62*, 241–302. [CrossRef]
62. Chen, F.; Gupta, N.; Behera, R.K.; Rohatgi, P.K. Graphene-Reinforced Aluminum Matrix Composites: A Review of Synthesis Methods and Properties. *JOM* **2018**, *70*, 837–845. [CrossRef]
63. Bardotti, L.; Jensen, P.; Hoareau, A.; Treilleux, M.; Cabaud, B. Experimental Observation of Fast Diffusion of Large Antimony Clusters on Graphite Surfaces. *Phys. Rev. Lett.* **1995**, *74*, 4694–4697. [CrossRef] [PubMed]
64. Galashev, A.Y.; Katin, K.P.; Maslov, M.M. Morse parameters for the interaction of metals with graphene and silicene. *Phys. Lett. A* **2019**, *383*, 252–258. [CrossRef]
65. Verkhovtsev, A.V.; Schramm, S.; Solov'yov, A.V. Molecular dynamics study of the stability of a carbon nanotube atop a catalytic nanoparticle. *Eur. Phys. J. D* **2014**, *68*. [CrossRef]
66. Sierra-Suarez, J.A.; Majumdar, S.; McGaughey, A.J.H.; Malen, J.A.; Higgs, C.F. Morse potential-based model for contacting composite rough surfaces: Application to self-assembled monolayer junctions. *J. Appl. Phys.* **2016**, *119*, 145306. [CrossRef]
67. Krylova, K.A.; Baimova, J.A.; Lobzenko, I.P.; Rudskoy, A.I. Crumpled graphene as a hydrogen storage media: Atomistic simulation. *Phys. B Condens. Matter* **2020**, *583*, 412020. [CrossRef]
68. Yang, Y.; Liu, M.; Zhou, S.; Ren, W.; Zhou, Q.; Zhang, W. Strengthening behaviour of continuous graphene network in metal matrix composites. *Carbon* **2021**, *182*, 825–836. [CrossRef]
69. Mendelev, M.; King, A. The interactions of self-interstitials with twin boundaries. *Philos. Mag.* **2013**, *93*, 1268–1278. [CrossRef]
70. Daw, M.S.; Baskes, M.I. Embedded-atom method: Derivation and application to impurities, surfaces, and other defects in metals. *Phys. Rev. B* **1984**, *29*, 6443–6453. [CrossRef]
71. Mishin, Y.; Mehl, M.J.; Papaconstantopoulos, D.A.; Voter, A.F.; Kress, J.D. Structural stability and lattice defects in copper:Ab initio, tight-binding, and embedded-atom calculations. *Phys. Rev. B* **2001**, *63*, 224106. [CrossRef]
72. Zhao, Y.; Peng, X.; Fu, T.; Sun, R.; Feng, C.; Wang, Z. MD simulation of nanoindentation on (001) and (111) surfaces of Ag–Ni multilayers. *Phys. E-Low-Dimens. Syst. Nanostruct.* **2015**, *74*, 481–488. [CrossRef]
73. Weng, S.; Ning, H.; Hu, N.; Yan, C.; Fu, T.; Peng, X.; Fu, S.; Zhang, J.; Xu, C.; Sun, D.; et al. Strengthening effects of twin interface in Cu/Ni multilayer thin films—A molecular dynamics study. *Mater. Des.* **2016**, *111*, 1–8. [CrossRef]
74. Weng, S.; Ning, H.; Fu, T.; Hu, N.; Zhao, Y.; Huang, C.; Peng, X. Molecular dynamics study of strengthening mechanism of nanolaminated graphene/Cu composites under compression. *Sci. Rep.* **2018**, *8*. [CrossRef] [PubMed]
75. Somlyai-Sipos, L.; Janovszky, D.; Sycheva, A.; Baumli, P. Investigation of the Melting Point Depression of Copper Nanoparticles. *IOP Conf. Ser. Mater. Sci. Eng.* **2020**, *903*, 012002. [CrossRef]
76. Safina, L.R.; Murzaev, R.T. Size of Metal Nanoparticles as a Decisive Factor in the Formation of Nickel-Graphene Composite: Molecular Dynamics. *J. Struct. Chem.* **2021**, *62*, 794–801. [CrossRef]